Supplementary Information.

Insights into the Crystal Packing Interactions of a 960-nm-emissive DNA-Stabilized Silver Nanocluster

Giacomo Romolini,[a,1] Hiroki Kanazawa,[b,1] Simon Wentzel Lind,[a] Cecilia Cerretani,[a] Christian Brinch Mollerup,[c] Letizia Liccardo,[a] Zhiyu Huang,[a] Leila Lo Leggio,[a] Vanessa Rück,[a] Jiro Kondo,[b,*] and Tom Vosch[a,*]

[a] Department of Chemistry, University of Copenhagen, Universitetsparken 5, DK-2100 Copenhagen, Denmark.

[b] Department of Materials and Life Sciences, Sophia University, 7-1 Kioi-cho, Chiyoda-ku, 102-8554 Tokyo, Japan.

[c] Department of Forensic Medicine, University of Copenhagen, Frederik V's Vej 11, DK-2100 Copenhagen, Denmark.

[1] Contributed equally.

Materials and Methods

1. Synthesis of mutations of DNA960-AgNCs

The oligonucleotides and nuclease-free water were purchased from Integrated DNA Technologies (IDT). $AgNO_3$ (≥ 99.998%), $NaBH_4$ (≥ 99.99%) and ammonium acetate (NH_4OAc, ≥98%) were purchased from Sigma Aldrich. All chemicals were used as received and dissolved in nuclease-free H_2O. DNA-AgNCs were synthesized by mixing a hydrated DNA solution with $AgNO_3$ in a 50 mM NH_4OAc solution (pH=7). After 15 minutes, a fresh solution of $NaBH_4$ was added. The concentrations of the components in the final mixture were 30 μM for the DNA, 240 μM $AgNO_3$ and 240 μM $NaBH_4$. The solution was stored in the fridge for 3 days before HPLC purification. Figure S1 shows the absorption spectrum of the as-synthesized solutions before HPLC purification.
For clarity, the DNA sequence of the mutants is as follows:

Mutant's name	Sequence
C8	5′-CCGCGCG**C**GCCGCGAA-3′
A8	5′-CCGCGCG**A**GCCGCGAA-3′
-C8	5′-CCGCGCGGCCGCGAA-3′
G8	5′-CCGCGCG**G**GCCGCGAA-3′
T8	5′-CCGCGCG**T**GCCGCGAA-3′
A3T8	5′-CC**A**CGCG**T**GCCGCGAA-3′
A3	5′-CC**A**CGCGCGCCGCGAA-3′

2. HPLC purification

The HPLC purification was performed with an Agilent Technologies 1260 Infinity fluorescence detector, an Agilent Technologies 1100 Series UV-Vis detector, a C18 column (Phenomenex), and a fraction collector. The mobile phase was gradually changed and made of a mixture of 35 mM triethylammonium acetate (TEAA) buffer in water (solvent A) and 35 mM TEAA in methanol (solvent B). The gradient was as follows:

Time	% B
0 min	5
2 min	5
27 min	30
30 min	95

The separation run was followed by 5 minutes at 95% B to remove any remaining sample from the column. Figure S2 shows the chromatograms of the 960-nm emissive DNA-AgNC. The retention time with the abovementioned method is between 23 and 25 minutes.
The DNA-AgNC sample was purified twice with the same HPLC method to improve the purity. The first run was performed using a LUNA C18 column (5 μm, 100 Å, 250 x 10 mm, Phenomenex) with a flow rate of 4.7 mL/min, while the second run was carried out with a Kinetex C18 column (5 μm, 100 Å, 250 x 4.6 mm, Phenomenex) with a flow rate of 1 mL/min. Afterwards, the purified DNA-AgNC solution was solvent-exchanged to 50 mM NH_4OAc with 3 kDa cut-off membrane filters (Amicon Ultra), depending on which NH_4OAc solution was used to synthesize the clusters. Figure S3 shows the absorption spectra after the first and second purification.

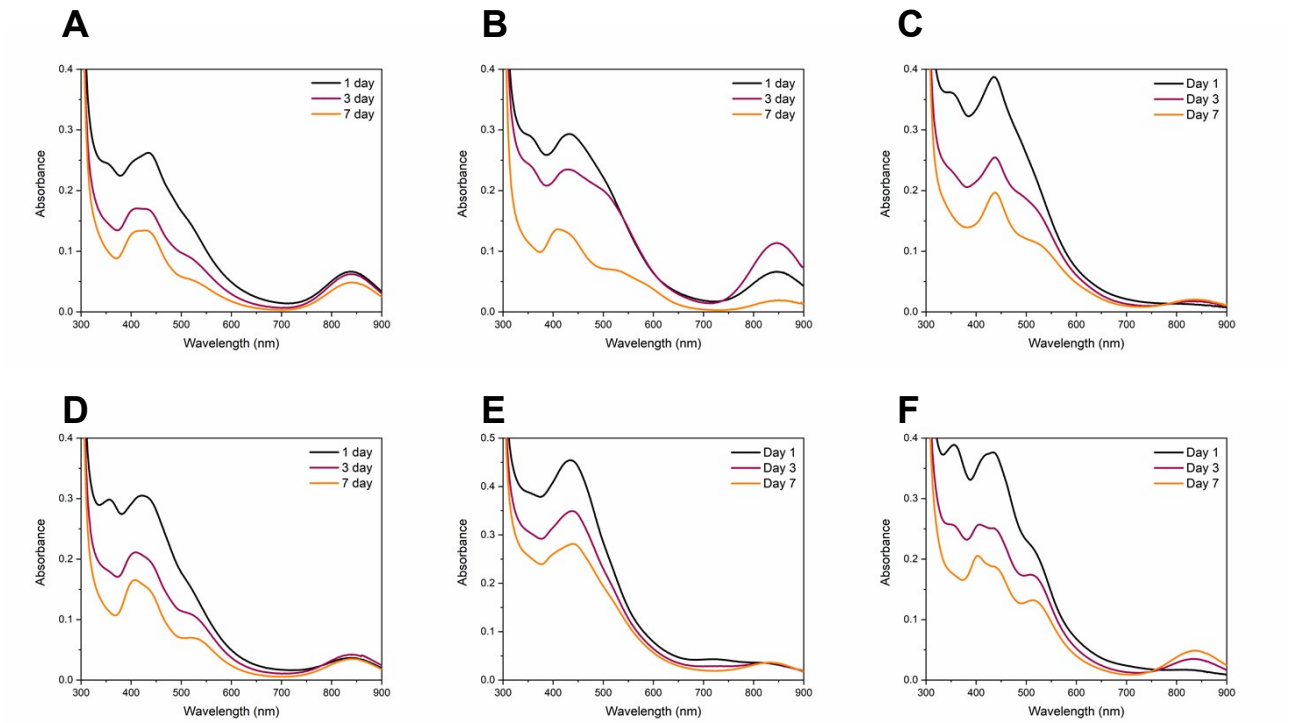

Figure S1. Absorption spectra of DNA960-AgNC mutants were measured on days 1, 3, and 7 to identify the optimal time for HPLC purification and maximize AgNC yield. Panels show individual mutants: (**A**) A8, (**B**) -C8, (**C**) G8, (**D**) T8, (**E**) A3T8, and (**F**) A3.

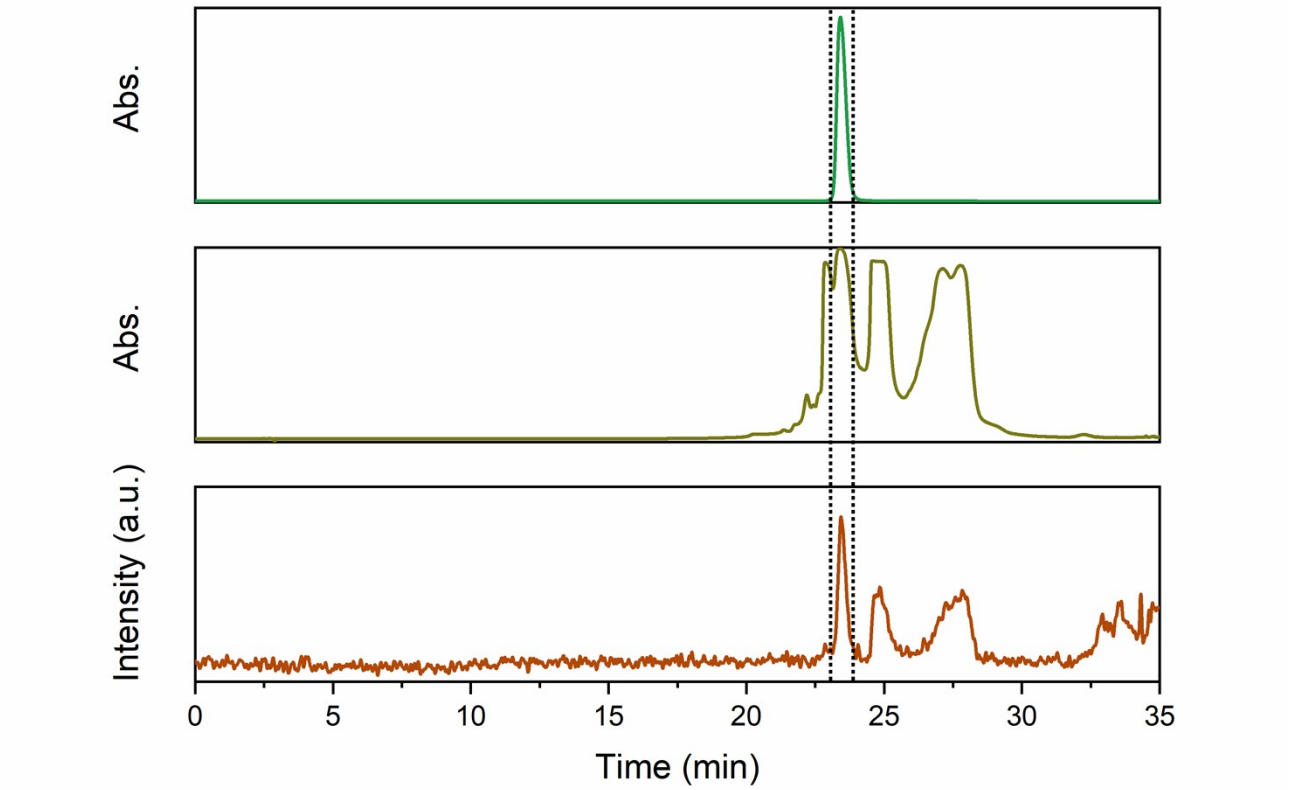

Figure S2. HPLC chromatograms of mutant A8, monitoring the absorbance at **A)** 830 nm and **B)** 260 nm. The absorbance is given in mOD. **C)** Chromatograms that monitor the emission at 900 nm, exciting at 830 nm. The dashed lines define the collected fraction.

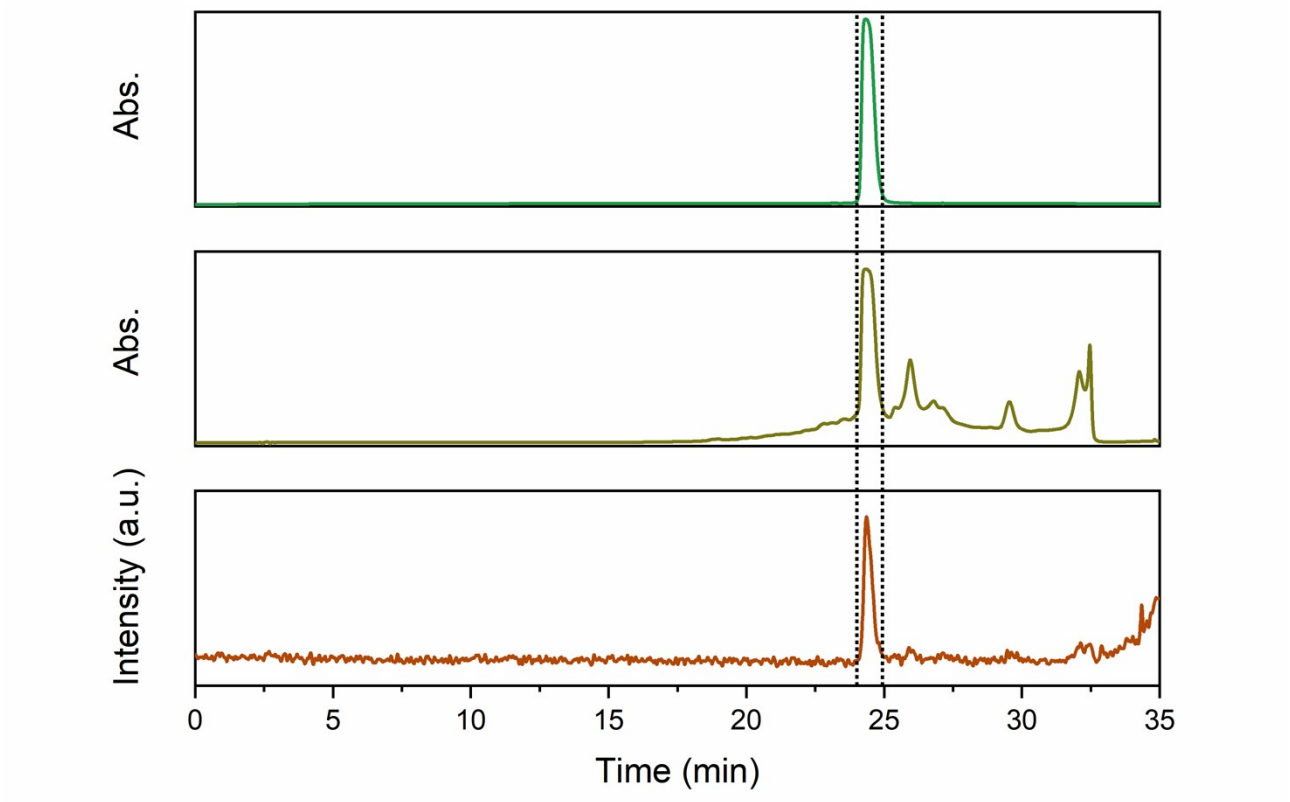

Figure S3. HPLC chromatograms of mutant -C8, monitoring the absorbance at **A)** 830 nm and **B)** 260 nm. The absorbance is given in mOD. **C)** Chromatograms that monitor the emission at 900 nm, exciting at 830 nm. The dashed lines define the collected fraction.

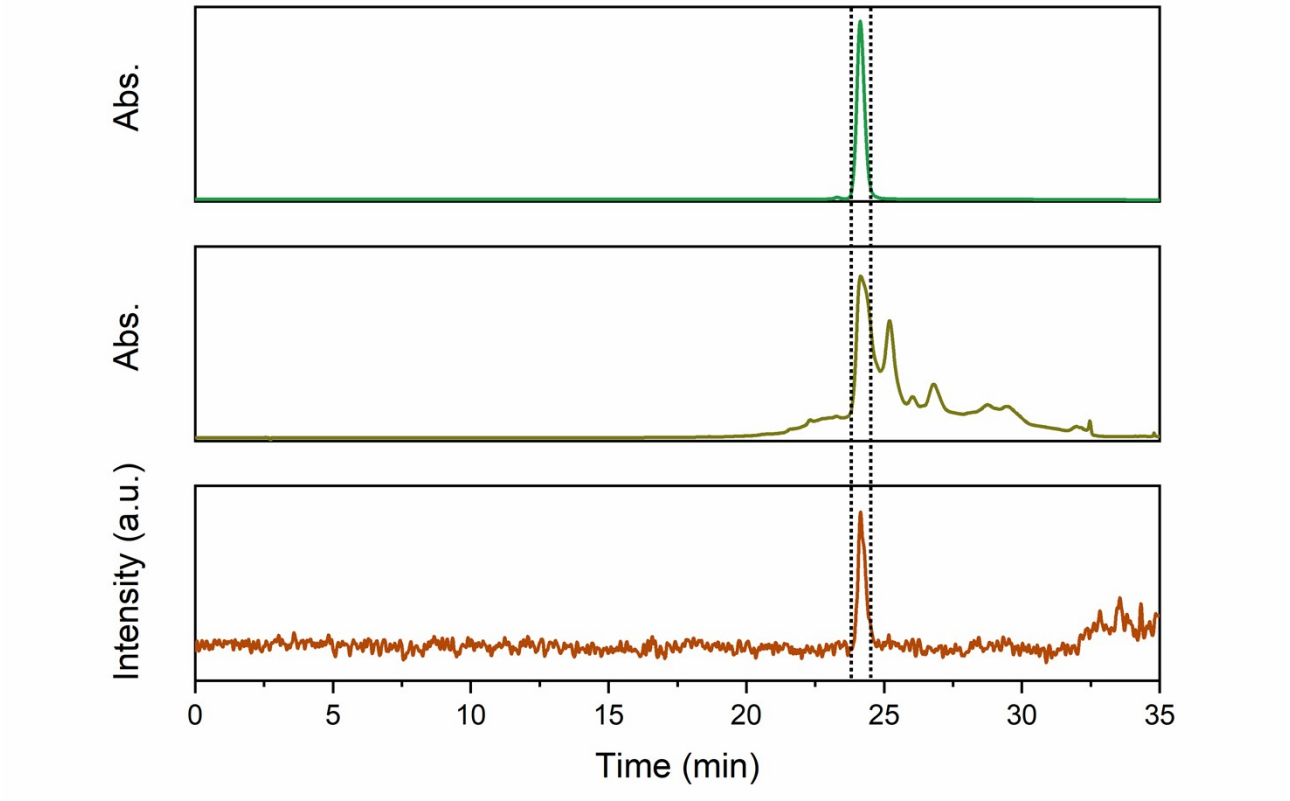

Figure S4. HPLC chromatograms of mutant G8, monitoring the absorbance at **A)** 830 nm and **B)** 260 nm. The absorbance is given in mOD. **C)** Chromatograms that monitor the emission at 900 nm, exciting at 830 nm. The dashed lines define the collected fraction.

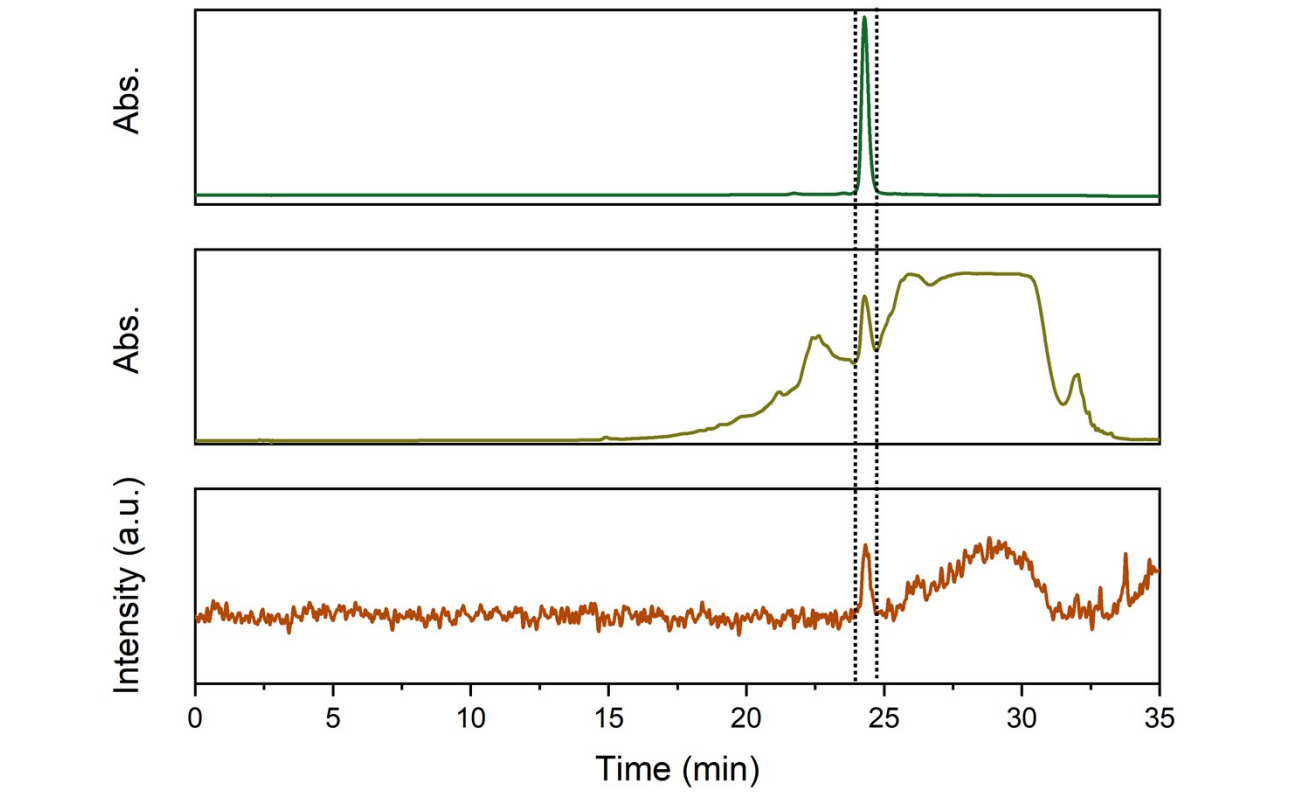

Figure S5. HPLC chromatograms of mutant T8, monitoring the absorbance at **A)** 830 nm and **B)** 260 nm. The absorbance is given in mOD. **C)** Chromatograms that monitor the emission at 900 nm, exciting at 830 nm. The dashed lines define the collected fraction.

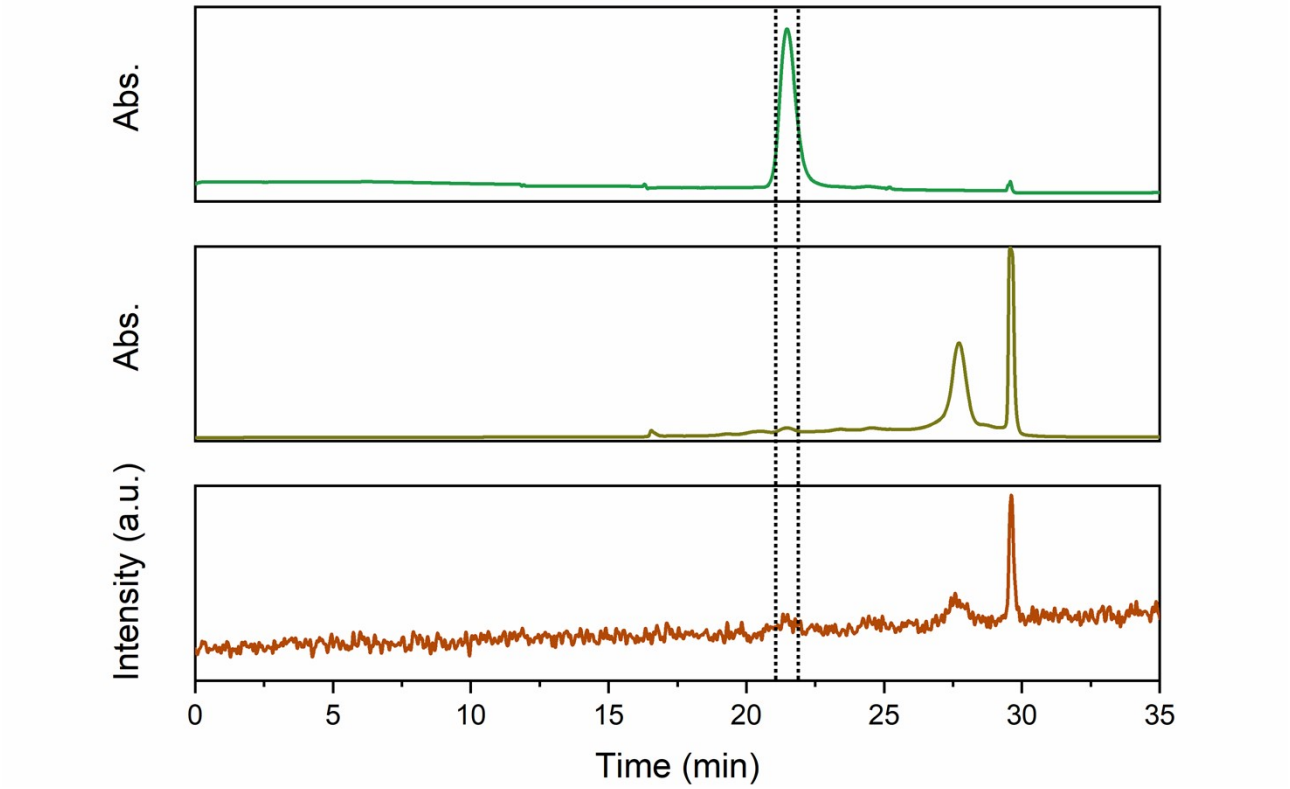

Figure S6. HPLC chromatograms of mutant A3T8, monitoring the absorbance at **A)** 830 nm and **B)** 260 nm. The absorbance is given in mOD. **C)** Chromatograms that monitor the emission at 900 nm, exciting at 830 nm. The dashed lines define the collected fraction.

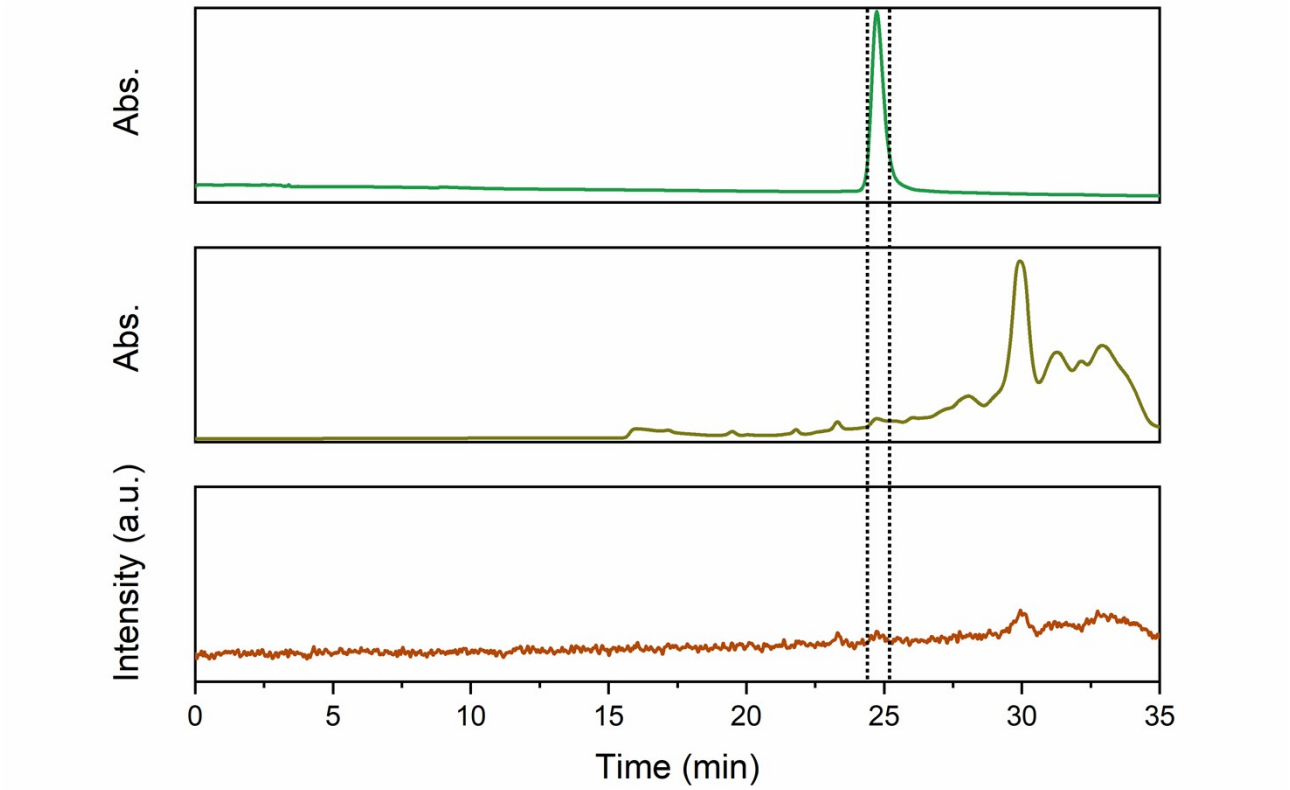

Figure S7. HPLC chromatograms of mutant A3, monitoring the absorbance at **A)** 830 nm and **B)** 260 nm. The absorbance is given in mOD. **C)** Chromatograms that monitor the emission at 900 nm, exciting at 830 nm. The dashed lines define the collected fraction.

3. Spectroscopic measurements in solution

3.1 Steady-state absorption measurements

Absorption spectra were measured with a LAMBDA 1050 UV/Vis/NIR spectrophotometer from Perkin Elmer using a deuterium lamp for ultraviolet radiation and a tungsten-halogen lamp for visible and near-infrared (NIR) radiation. All measurements were performed in a single-beam configuration with a "zero/baseline" correction, *i.e.*, measuring the 100%/0% transmittance with air as reference. The corresponding solvent spectra were measured separately and then subtracted from the samples' spectra. The absorbance of the samples was kept below 0.1 to avoid inner filter effects during emission measurements.

3.2 Fluorescence spectra and decay time measurements on a home-build microscope

Emission spectra and decay time measurements were performed on our home-built confocal microscope.[1] A pulsed continuum white-light laser (SuperK EXTREME EXB-6, NKT Photonics) was used as an excitation source delivering a wavelength of 790 nm by sending the continuum output through an acousto-optic tunable filter (SuperK SELECT, NKT Photonics). A repetition rate of 11.13 MHz was used for the time-resolved measurements and 77.88 MHz for the steady-state measurements. The output of the laser was expanded and collimated by a lens system and cleaned up by an 800 nm short-pass filter (FESH0800, Thorlabs) before it was reflected by a 30:70 beam splitter (XF122, Omega Optical) and sent through an objective. For the decays shown in Figure S8 through S13, an oil immersion objective (UPlanSApo 100x, NA = 1.4, Olympus) was used, while for the quantum yield and emission spectra (Figure S4) an air objective (CPlanFLN 10x, NA = 0.3, Olympus) was utilized. The objective that collected the fluorescence was directed through a 100 µm pinhole

and an 815 nm long-pass filter (HQ815LP, Chroma). The fluorescence was then sent through a spectrograph (SP 2356 spectrometer, 300 grooves/mm, Acton Research) onto a nitrogen cooled CCD camera (SPEC-10:100B/LN-eXcelon, Princeton Instruments) for the recording of spectra. Finally, the emission spectra were wavelength and intensity corrected as reported previously.[1]

For the quantum yield measurements, standard 1 cm quartz cuvettes (Hellma) were filled with either the blank (50 mM NH_4OAc; used for subtracting residual laser scatter), a solution of the 960-nm emissive DNA-AgNC, or a solution of the reference (see section 3.3). The cuvettes were placed on top of the microscope's sample stage, and the laser was focused around 1 mm into the solutions ensuring that the spectra were recorded under identical conditions.

The fluorescence decays were fitted with FluoFit 4.6 software (PicoQuant) using a single exponential reconvolution model, including the instrument response function (IRF) to obtain a good fit.

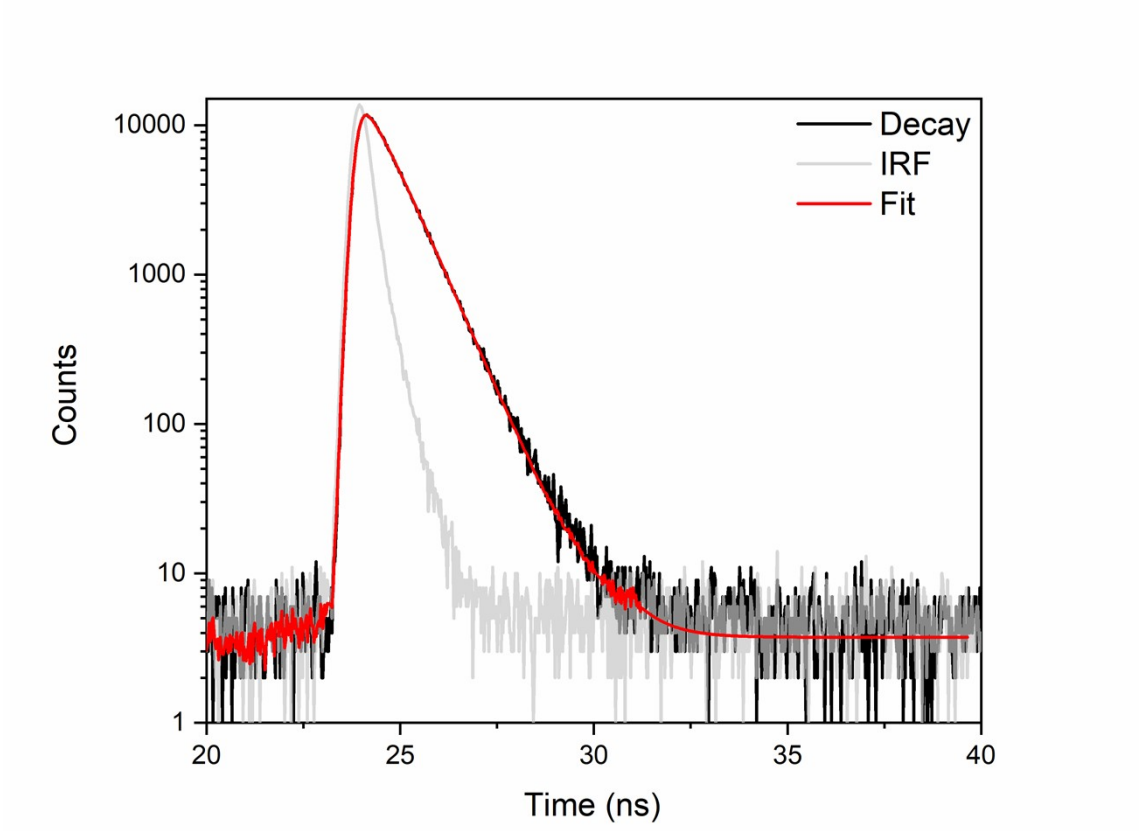

Figure S8. Fluorescence decay curves of the DNA960-AgNC A8 mutant in solution, exciting at 790 nm. The gray curve is the instrument response function.

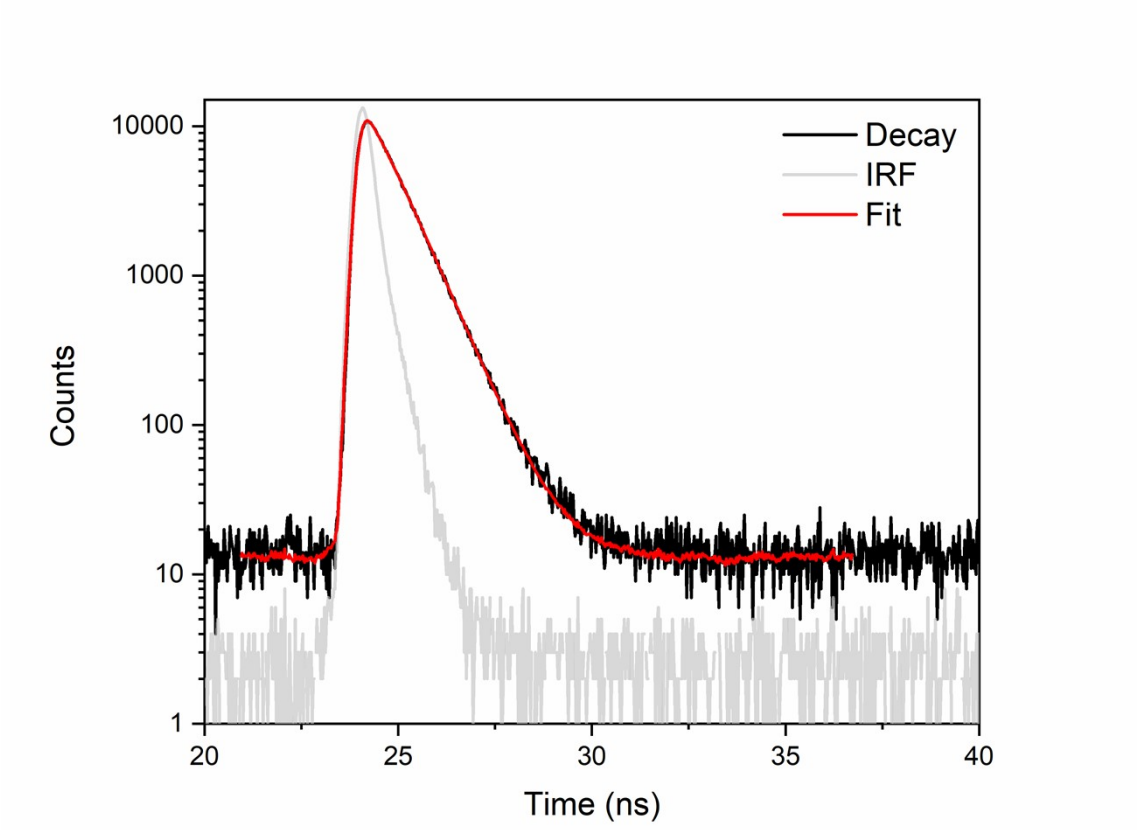

Figure S9. Fluorescence decay curves of the DNA960-AgNC -C8 mutant in solution, exciting at 790 nm. The gray curve is the instrument response function.

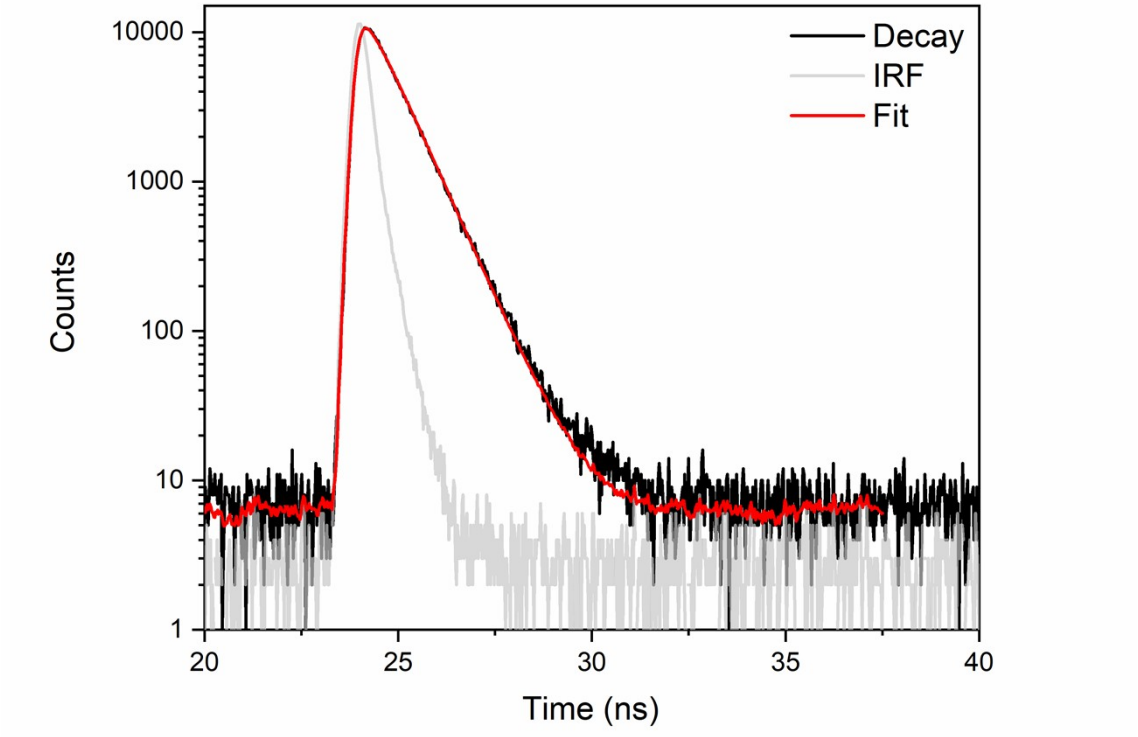

Figure S10. Fluorescence decay curves of the DNA960-AgNC G8 mutant in solution exciting at 790 nm. The gray curve is the instrument response function.

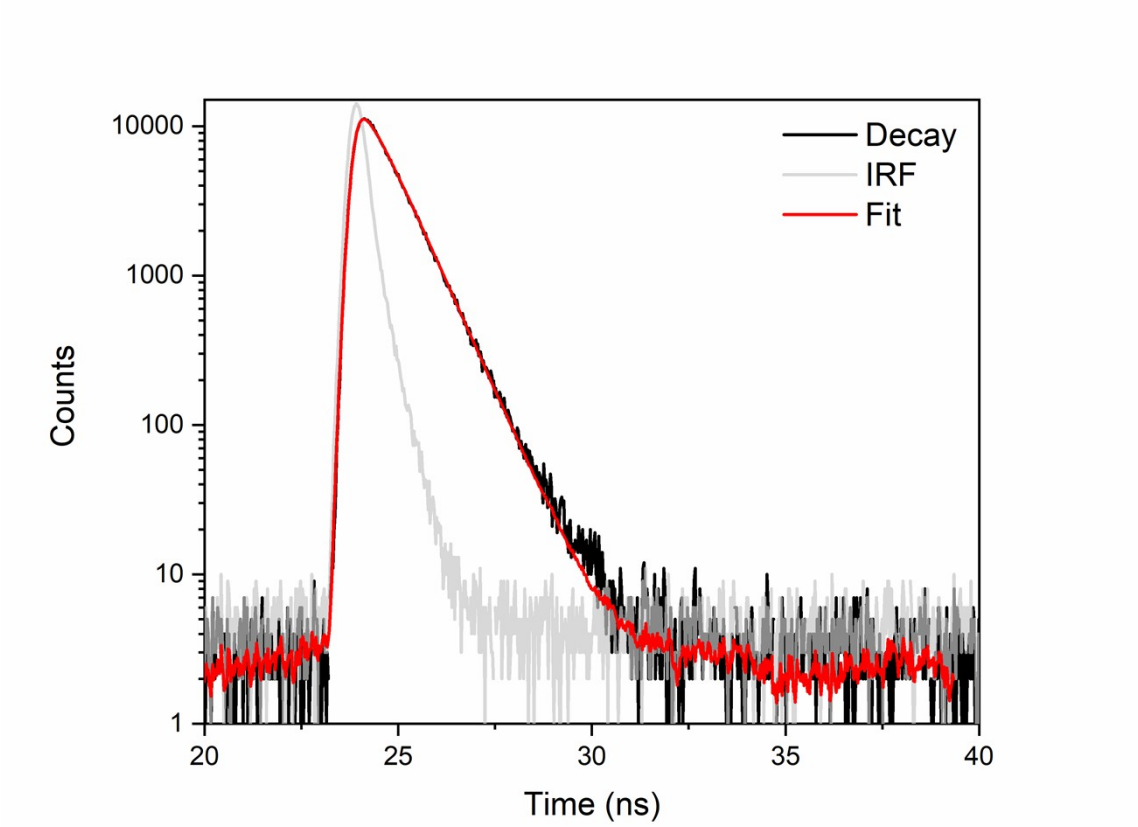

Figure S11. Fluorescence decay curves of the DNA960-AgNC T8 mutant in solution exciting at 790 nm. The gray curve is the instrument response function.

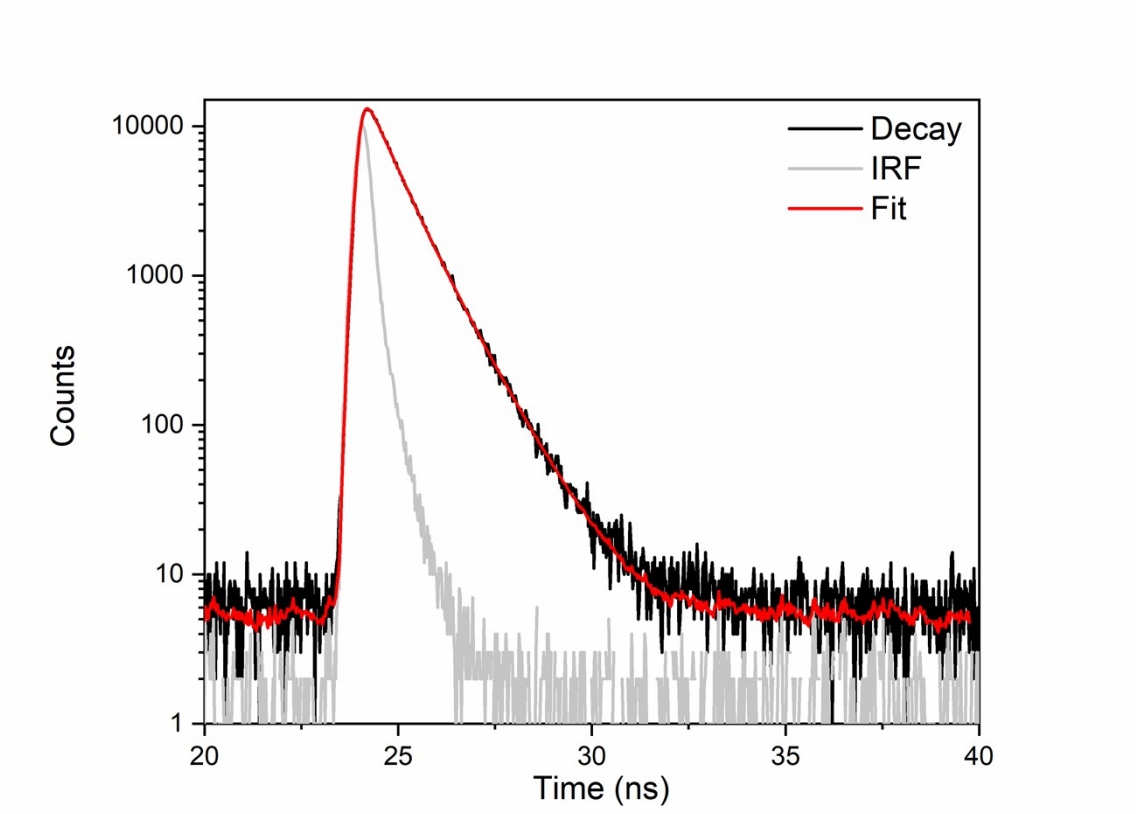

Figure S12. Fluorescence decay curves of the DNA960-AgNC A3T8 mutant in solution exciting at 790 nm. The gray curve is the instrument response function.

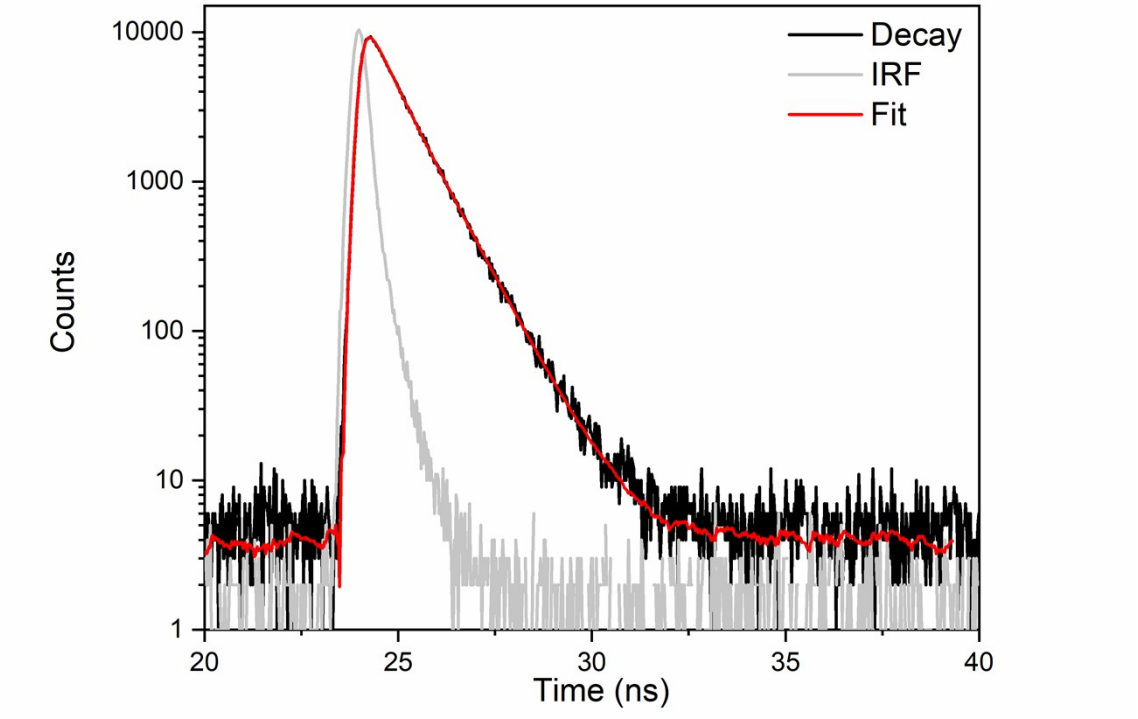

Figure S13. Fluorescence decay curves of the DNA960-AgNC A3 mutant in solution exciting at 790 nm. The gray curve is the instrument response function.

3.3 Quantum yield determination

The quantum yield of all mutations was determined in 50 mM NH_4OAc aqueous solution at room temperature, using C8 in the same medium as reference (QY_{ref} = 0.12).[2] Absorption and emission spectra were measured at one concentration for all the mutations and the reference. The quantum yield was then calculated according to equation 1:[3]

$$QY = \frac{F_{DNA-AgNC}}{f_{A,DNA-AgNC}} \cdot \frac{f_{A,ref}}{F_{ref}} \cdot \frac{n_{DNA-AgNC}^{2}}{n_{ref}^{2}} \cdot QY_{ref} \qquad \text{Equation 1}$$

Where *QY* represents the quantum yield of the individual mutation, *F* is the integrated emission spectrum (*i.e.*, the area under the fluorescence spectrum), f_A defines the fraction of absorbed light at the excitation wavelength (790 nm), and *n* is the refractive index of the medium where the compounds are dissolved. The subscripts *DNA-AgNC* and *ref* indicate the DNA-AgNC investigated in this study and C8, respectively.
The absorption and emission spectra of both DNA-AgNCs are reported in Figure S14.

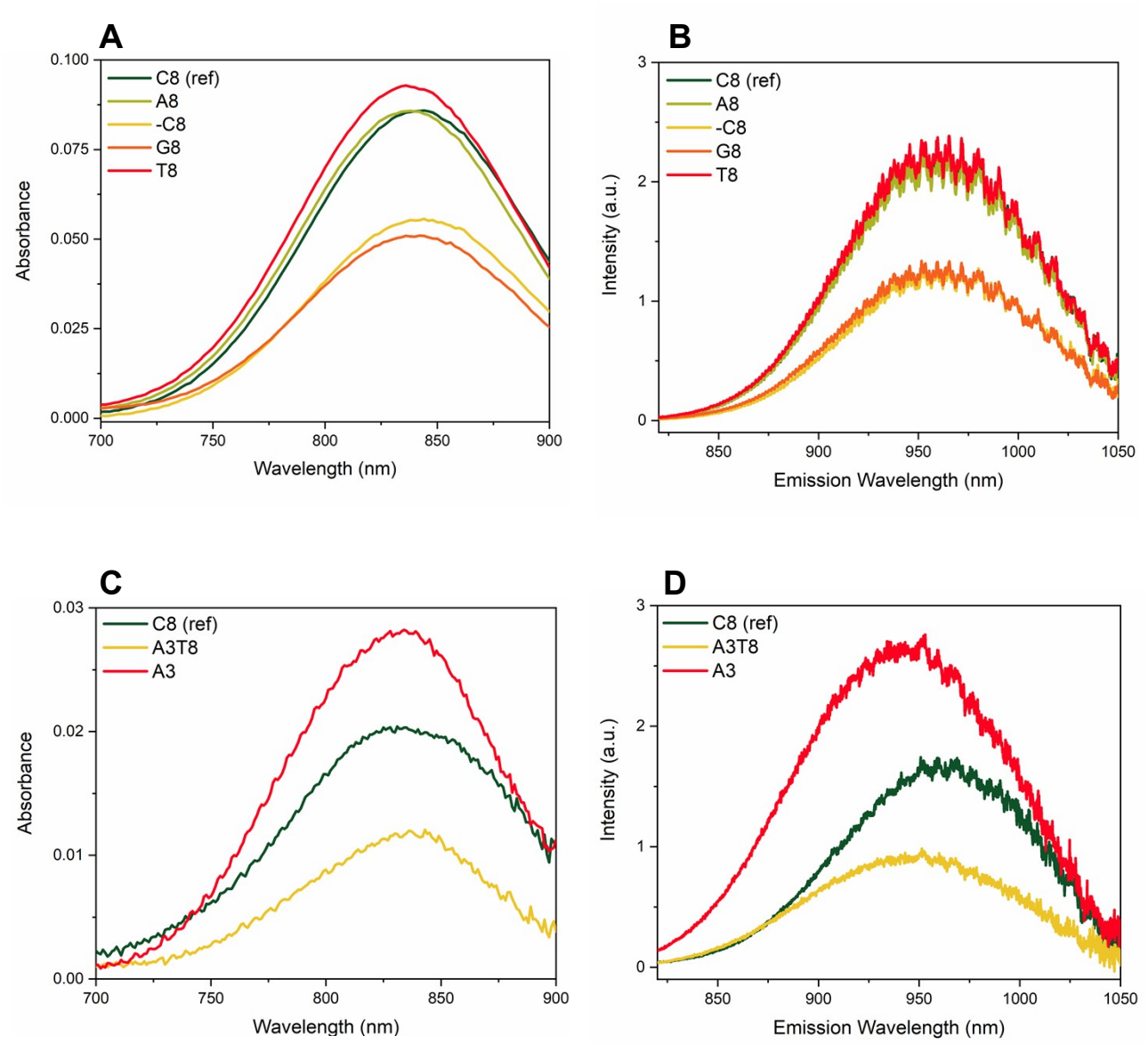

Figure S14. Quantum Yield data. (**Left)** Absorption spectra and (**Right)** emission spectra of DNA960-AgNC (reference) and the mutations (sample) measured in 50 mM NH_4OAc at room temperature. The emission spectra were recorded by exciting at 790 nm.

4. Electrospray ionization-Mass Spectrometry (ESI-MS).

The ESI-MS data were acquired with a Xevo G2-XS QTof (Waters Corporation), using negative ion mode with a 1.5 kV capillary voltage, 30 V cone voltage, 80 V source offset and collision mode set to off. Spectra were collected from m/z 750 to 4000, with a scan time of 1 s. The source temperature was 100 °C with a cone gas flow of 50 L/h, and the desolvation temperature and gas flow were 350 °C and 800 L/h, respectively. The QTOF was calibrated using ESI-L Low Tune Mix (Agilent Technologies), which contained compounds for negative mode in the mass range of m/z 113 to 2834. The sample was injected using an Acquity I-Class Plus system (Waters) with a flow-through needle autosampler, with a flow of 0.05 mL/min 50 mM NH_4OAc at pH 7 MeOH (80:20) and using 3 μL injection volume. The system was operated using UNIFI v.1.9.4 (Waters), and the final spectra were generated by averaging multiple spectra surrounding the apex of the observed peak. The recorded data were analyzed and fitted with the open-source software enviPat.[4]

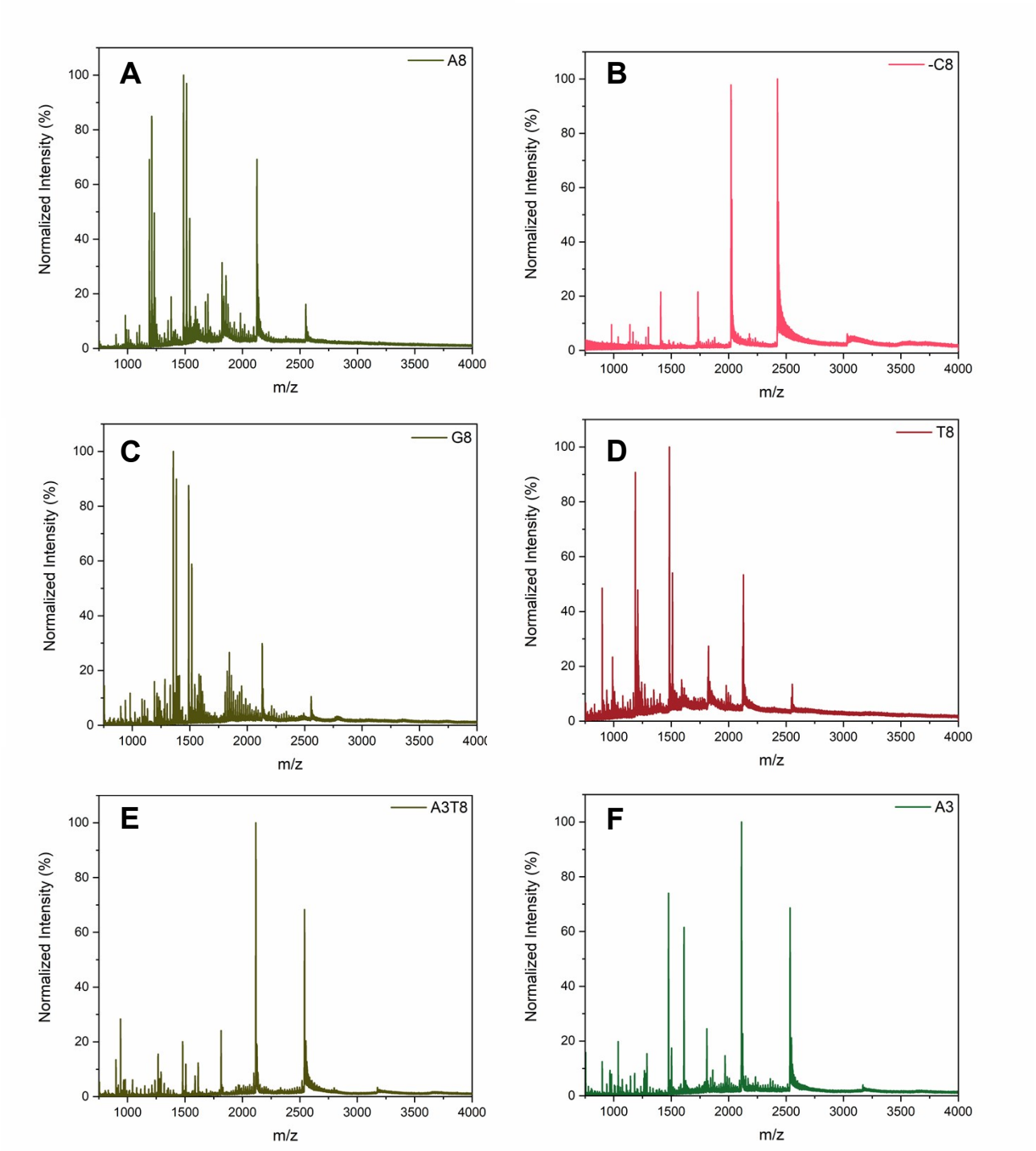

Figure S15. Mass spectra of DNA960-AgNC mutations. Mass spectra of **A**) A8, **B**) -C8, **C**) G8, **D**) T8, **E**) A3T8, and **F**) A3 in 50 mM NH_4OAc.

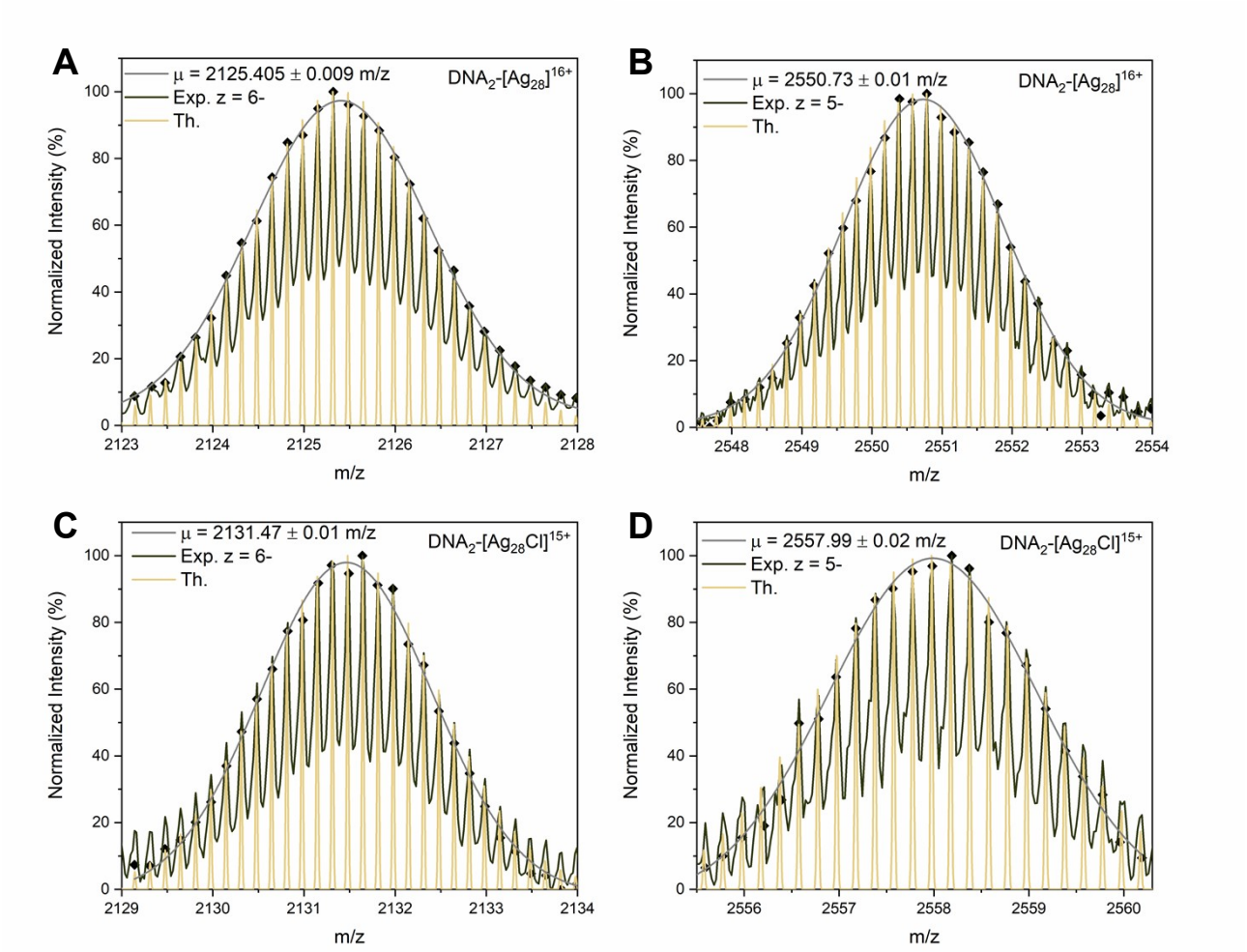

Figure S16. Zoomed-in view of the mass spectrum reported in Figure S15A of the A8 mutation. **A**) and **C**) Molecular ion peak with z=6$^-$ charge state. The experimental isotopic distribution is reported with the corresponding Gaussian fit (gray) and the theoretical isotopic distribution in sand color (**A**) for DNA_2-$[Ag_{28}]^{16+}$ and (**C**) DNA_2-$[Ag_{28}Cl]^{15+}$. The experimental average masses are *m/z* 2125.405±0.009 and 2131.47±0.01, respectively. **B**) and **D**) Molecular ion peak with z=5$^-$ charge state. The experimental isotopic distribution is reported with the corresponding Gaussian fit (gray) and the theoretical isotopic distribution in sand color (**B**) for DNA_2-$[Ag_{28}]^{16+}$ and (**D**) purple for DNA_2-$[Ag_{28}Cl]^{15+}$. The experimental average masses are *m/z* 2550.73±0.01 and 2557.99±0.02, respectively. See Table S2 for the calculations.

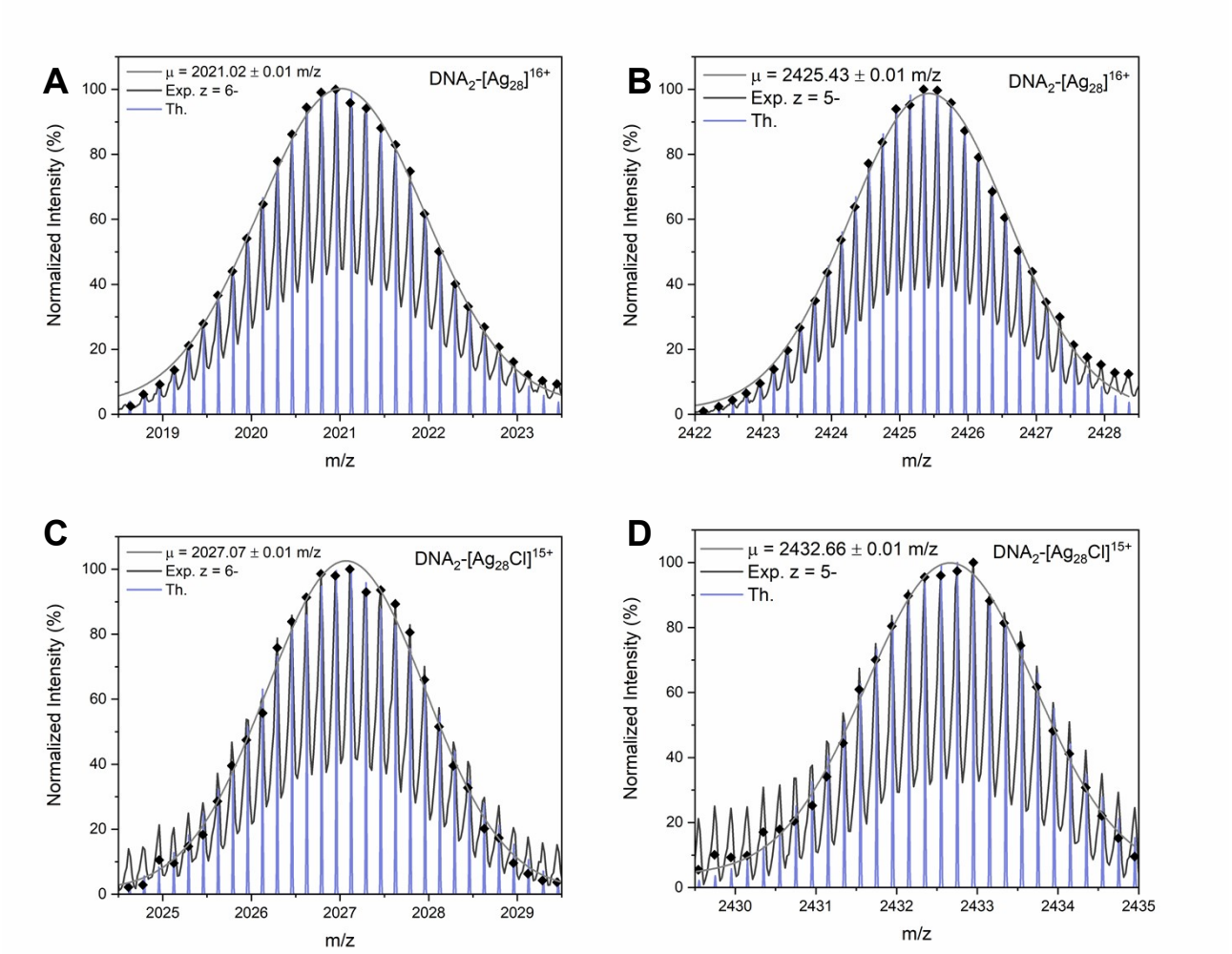

Figure S17. Zoomed-in view of the mass spectrum reported in Figure S15B of the -C8 mutation. **A**) and **C**) Molecular ion peak with z=6$^-$ charge state. The experimental isotopic distribution is reported with the corresponding Gaussian fit (gray) and the theoretical isotopic distribution in sand color (**A**) for DNA_2-$[Ag_{28}]^{16+}$ and (**C**) DNA_2-$[Ag_{28}Cl]^{15+}$. The experimental average masses are *m/z* 2021.02±0.01 and 2027.07±0.01, respectively. **B**) and **D**) Molecular ion peak with z=5$^-$ charge state. The experimental isotopic distribution is reported with the corresponding Gaussian fit (gray) and the theoretical isotopic distribution in sand color (**B**) for DNA_2-$[Ag_{28}]^{16+}$ and (**D**) purple for DNA_2-$[Ag_{28}Cl]^{15+}$. The experimental average masses are *m/z* 2425.43±0.01 and 2432.66±0.01, respectively. See Table S2 for the calculations.

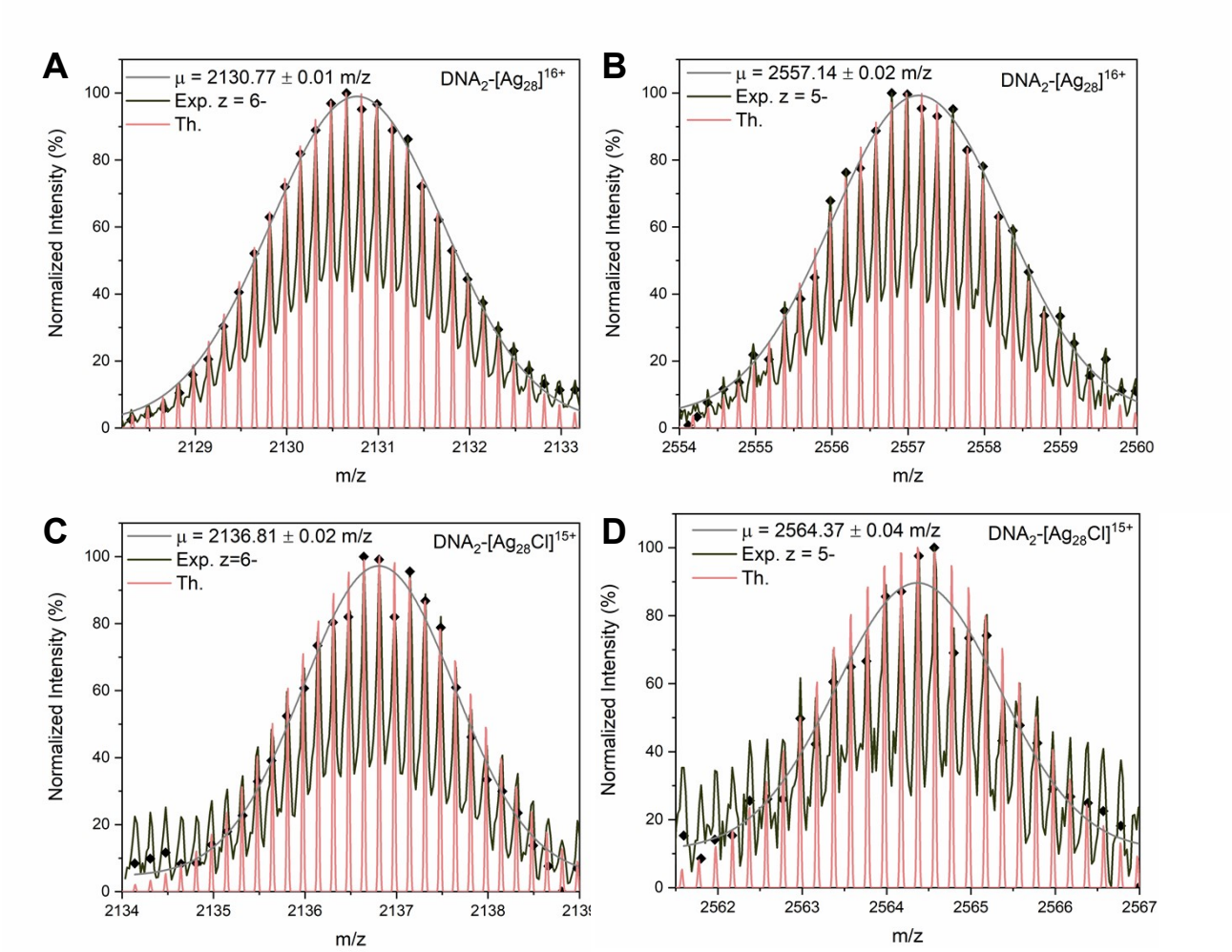

Figure S18. Zoomed-in view of the mass spectrum reported in Figure S15C of the G8 mutation. **A**) and **C**) Molecular ion peak with z=6$^-$ charge state. The experimental isotopic distribution is reported with the corresponding Gaussian fit (gray) and the theoretical isotopic distribution in sand color (**A**) for DNA_2-$[Ag_{28}]^{16+}$ and (**C**) DNA_2-$[Ag_{28}Cl]^{15+}$. The experimental average masses are *m/z* 2130.77±0.01 and 2136.81±0.02, respectively. **B**) and **D**) Molecular ion peak with z=5$^-$ charge state. The experimental isotopic distribution is reported with the corresponding Gaussian fit (gray) and the theoretical isotopic distribution in sand color (**B**) for DNA_2-$[Ag_{28}]^{16+}$ and (**D**) purple for DNA_2-$[Ag_{28}Cl]^{15+}$. The experimental average masses are *m/z* 2557.14±0.02 and 2564.37±0.04, respectively. See Table S2 for the calculations.

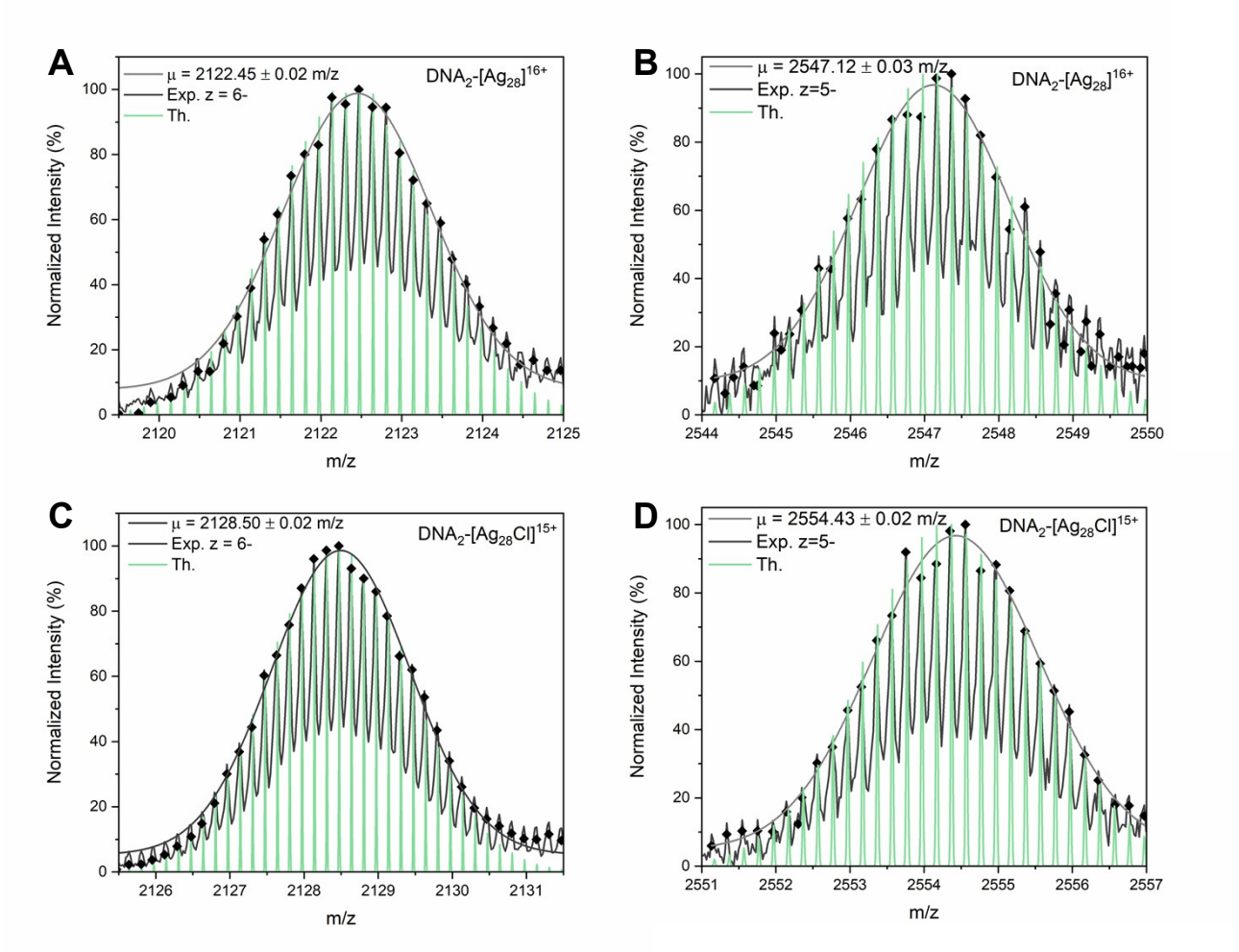

Figure S19. Zoomed-in view of the mass spectrum reported in Figure S15D of the T8 mutation. **A**) and **C**) Molecular ion peak with z=6$^-$ charge state. The experimental isotopic distribution is reported with the corresponding Gaussian fit (gray) and the theoretical isotopic distribution in sand color (**A**) for DNA_2-$[Ag_{28}]^{16+}$ and (**C**) DNA_2-$[Ag_{28}Cl]^{15+}$. The experimental average masses are *m/z* 2122.45±0.02 and 2128.50±0.02, respectively. **B**) and **D**) Molecular ion peak with z=5$^-$ charge state. The experimental isotopic distribution is reported with the corresponding Gaussian fit (gray) and the theoretical isotopic distribution in sand color (**B**) for DNA_2-$[Ag_{28}]^{16+}$ and (**D**) purple for DNA_2-$[Ag_{28}Cl]^{15+}$. The experimental average masses are *m/z* 2547.14±0.03 and 2554.43±0.02, respectively. See Table S2 for the calculations.

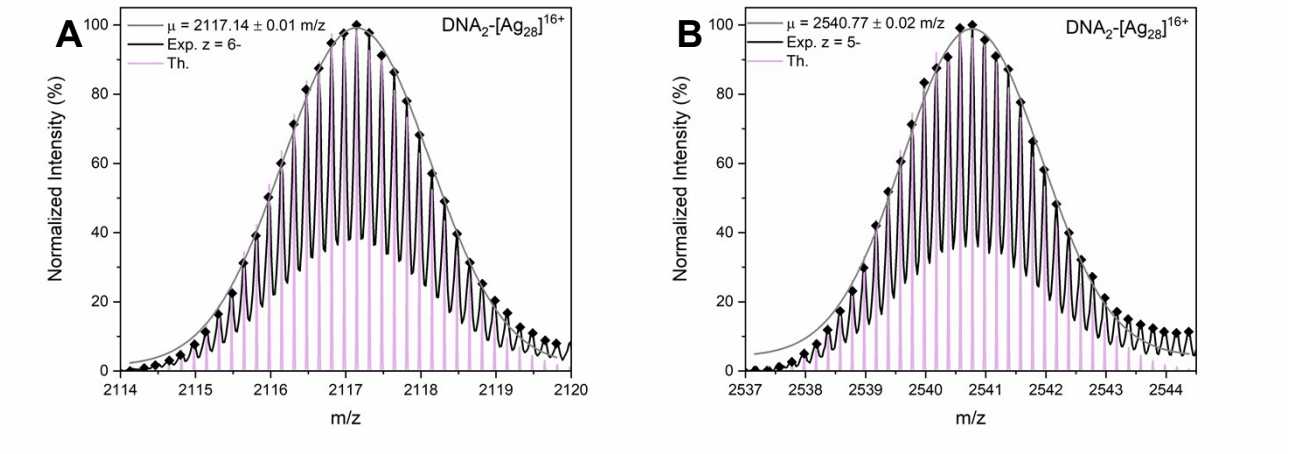

Figure S20. Zoomed-in view of the mass spectrum reported in Figure S15E of the A3T8 mutation. The experimental isotopic distribution is reported with the corresponding Gaussian fit (gray) and the theoretical isotopic distribution in light purple color (**A**) for DNA_2-$[Ag_{28}]^{16+}$ and $z=6^-$, and (**B**) for DNA_2-$[Ag_{28}]^{16+}$ and $z=5^-$. The experimental average masses are *m/z* 2117.14±0.01 and 2540.77±0.02, respectively. See Table S2 for the calculations.

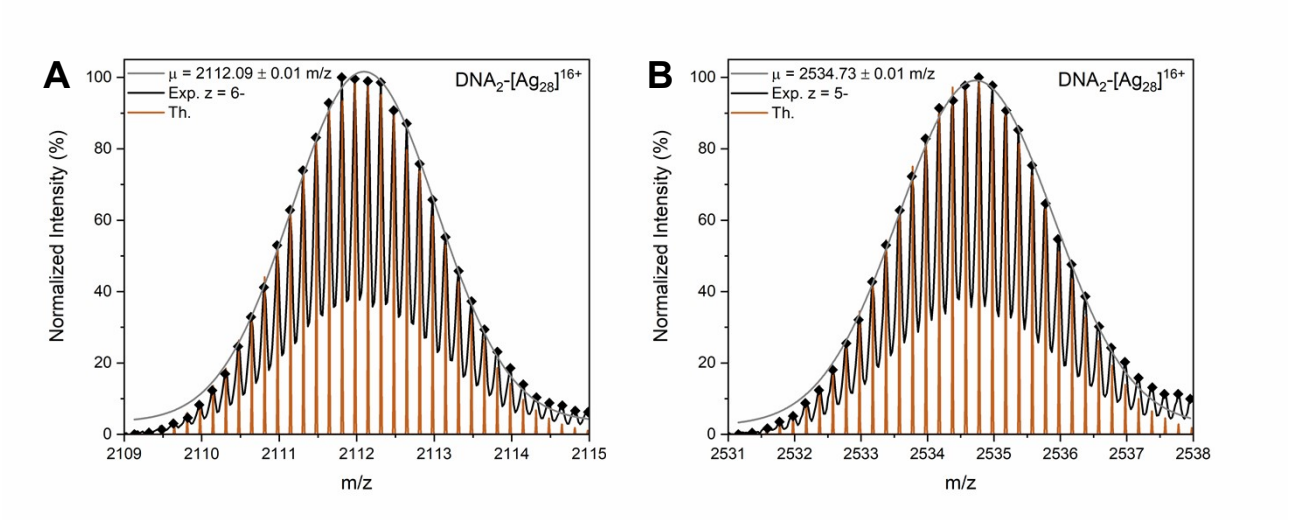

Figure S21. Zoomed-in view of the mass spectrum reported in Figure S15F of the A3 mutation. The experimental isotopic distribution is reported with the corresponding Gaussian fit (gray) and the theoretical isotopic distribution in light brown color (**A**) for DNA_2-$[Ag_{28}]^{16+}$ and $z=6^-$, and (**B**) for DNA_2-$[Ag_{28}]^{16+}$ and $z=5^-$. The experimental average masses are *m/z* 2112.09±0.01 and 2534.73±0.01, respectively. See Table S2 for the calculations.

	Molecular formula	z	Chemical Formula	Exact Mass*	Molecular Weight*	x_0^{th}	x_0^{exp}	error
A8	DNA_2-$[Ag_{28}]^{16+}$	5-	$C_{306}H_{386}N_{132}O_{182}P_{30}[Ag_{28}]^{16+}$	12743.06 amu	12774.72 g/mol	2550.681 ± 0.002	2550.73 ± 0.01	**+ 0.049**
		6-	$C_{306}H_{386}N_{132}O_{184}P_{30}[Ag_{28}]^{16+}$			2125.400 ± 0.001	2125.405± 0.009	**+ 0.005**
	DNA_2-$[Ag_{28}Cl]^{15+}$	5-	$C_{306}H_{386}N_{132}O_{182}P_{30}[Ag_{28}]^{16+}Cl^-$	12778.025 amu	12810.17 g/mol	2557.972 ± 0.002	2557.99 ± 0.02	**+ 0.018**
		6-	$C_{306}H_{386}N_{132}O_{182}P_{30}[Ag_{28}]^{16+}Cl^-$			2131.4948 ± $8{\cdot}10^{-4}$	2131.47 ± 0.01	**+ 0.025**
-C8	DNA_2-$[Ag_{28}]^{16+}$	5-	$C_{286}H_{362}N_{122}O_{172}P_{28}[Ag_{28}]^{16+}$	12116.94 amu	12148.30 g/mol	2425.396 ± 0.002	2425.43 ± 0.01	**+ 0.034**
		6-	$C_{286}H_{362}N_{122}O_{172}P_{28}[Ag_{28}]^{16+}$			2021.001 ± 0.001	2021.02± 0.01	**+ 0.019**
	DNA_2-$[Ag_{28}Cl]^{15+}$	5-	$C_{286}H_{362}N_{122}O_{172}P_{28}[Ag_{28}]^{16+}Cl^-$	12151.91 amu	12183.75 g/mol	2432.685 ± 0.004	2432.66 ± 0.01	**- 0.025**
		6-	$C_{286}H_{362}N_{122}O_{172}P_{28}[Ag_{28}]^{16+}Cl^-$			2027.070 ± 0.004	2027.07 ± 0.01	**+ 0.0**
G8	DNA_2-$[Ag_{28}]^{16+}$	5-	$C_{306}H_{386}N_{132}O_{184}P_{30}[Ag_{28}]^{16+}$	12775.05 amu	12806.72 g/mol	2557.081 ± 0.002	2557.14 ± 0.02	**+ 0.059**
		6-	$C_{304}H_{386}N_{132}O_{184}P_{30}[Ag_{28}]^{16+}$			2130.733 ± 0.001	2130.77± 0.01	**+ 0.037**
	DNA_2-$[Ag_{28}Cl]^{15+}$	5-	$C_{304}H_{386}N_{132}O_{184}P_{30}[Ag_{28}]^{16+}Cl^-$	12810.01 amu	12842.17 g/mol	2564.377 ± 0.001	2564.37 ± 0.04	**- 0.007**
		6-	$C_{304}H_{386}N_{132}O_{184}P_{30}[Ag_{28}]^{16+}Cl^-$			2136.801 ± 0.001	2136.81 ± 0.02	**+ 0.009**
	DNA_2-	5-	$C_{306}H_{388}N_{126}O_{186}P_{30}[Ag_{28}]^{16+}$	12725.03	12756.69	2547.077 ± 0.004	2547.12 ± 0.03	**+ 0.043**

		6-	$C_{306}H_{388}N_{126}O_{186}P_{30}[Ag_{28}]^{16+}$			2122.390 ± 0.004	2122.45± 0.02	**+ 0.06**
	DNA_2-$[Ag_{28}Cl]^{15+}$	5-	$C_{306}H_{388}N_{126}O_{186}P_{30}[Ag_{28}]^{16+}Cl^-$	12760.00 amu	12792.14 g/mol	2554.362 ± 0.004	2554.43 ± 0.02	**+ 0.068**
		6-	$C_{306}H_{388}N_{126}O_{186}P_{30}[Ag_{28}]^{16+}Cl^-$			2128.467 ± 0.004	2128.50 ± 0.02	**+ 0.033**
A3T8	DNA_2-$[Ag_{28}]^{16+}$	5-	$C_{306}H_{388}N_{126}O_{184}P_{30}[Ag_{28}]^{16+}$	12693.04 amu	12724.61 g/mol	2540.674 ± 0.004	2540.77 ± 0.02	**+0.096**
		6-	$C_{306}H_{388}N_{126}O_{184}P_{30}[Ag_{28}]^{16+}$			2117.059 ± 0.003	2117.14 ± 0.01	**+0.081**
A3	DNA_2-$[Ag_{28}]^{16+}$	5-	$C_{304}H_{386}N_{128}O_{182}P_{30}[Ag_{28}]^{16+}$	12663.04 amu	12694.59 g/mol	2534.668 ± 0.004	2534.73 ± 0.01	**+0.062**
		6-	$C_{304}H_{386}N_{128}O_{182}P_{30}[Ag_{28}]^{16+}$			2112.0556 ± 0.003	2112.09 ± 0.01	**+0.034**

Table S2. Center of Gaussian fits, x_0, for the experimentally measured mass spectra (x_0^{exp}) shown in Figures 2, S16-S21, and the corresponding theoretical mass distributions (x_0^{th}). The last column corresponds to the absolute error calculated as x_0^{exp}- x_0^{th}.
* As determined by ChemDraw Pro 8.0

5. Crystal data

5.1 Crystallization

Crystals were grown in an incubator at 293 K by the hanging drop vapor diffusion method. 0.2-1 µL of DNA-AgNC solution, with [DNA] ≈ 250 µM, were mixed with 0.2-1 µL of crystallization buffer and equilibrated against 250 µL of a reservoir solution, either 40% 2-methyl-2,4-pentanediol (MPD) or 40% polyethylene glycol (PEG) 3350. The crystallization buffer contains either 10% MPD or 10% PEG 3350, a nitrate salt (Li^+, Na^+, K^+, NH_4^+, Mg^{2+}, Ca^{2+} or Sr^{2+}) with different concentrations (10, 100, 200, 300, 400 and 500 mM), 10 mM spermine and 50 mM 3-(N-morpholino)propanesulfonic acid (MOPS) at pH 7. Crystals were obtained between 1 and 4 weeks after starting the crystallization. Examples are reported in Figure S22.

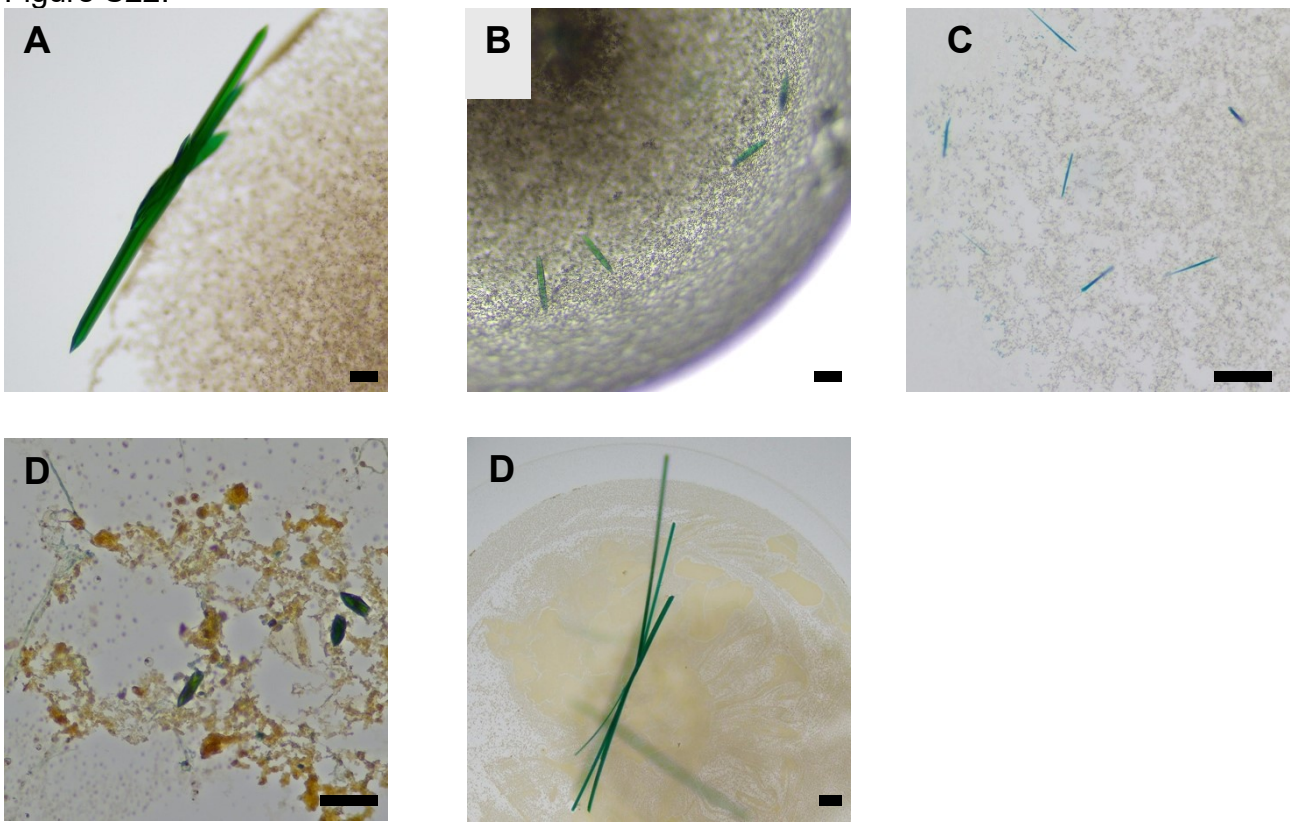

Figure S22. Examples of crystals. (**A**) A8 grown in 10% MPD, 10 mM spermine, 50 mM MOPS (pH 7) and 10 mM $NaNO_3$. (**B**) -C8 grown in 10% PEG, 10 mM spermine, 50 mM MOPS (pH 7) and 200 mM $NaNO_3$. (**C**) G8 grown in 10% MPD, 10 mM spermine, 50 mM MOPS (pH 7) and 200 mM NH_4NO_3. (**D**) T8 grown in 10% MPD, 10 mM spermine, 50 mM MOPS (pH 7) and 400 mM $Ca(NO_3)_2$. (**E**) A3T8 grown in 10% MPD, 10 mM spermine, 50 mM MOPS (pH 7) and 200 mM NH_4NO_3. The scale bar is 0.1 mm in all images.

5.2 Fluorescence spectra and decay time measurements of crystals on superconducting nanowire single photon detector setup

To properly measure the spectral features and decay times of DNA_2-$[Ag_{28}Cl_2]^{14+}$ crystals within the NIR II region, we utilized our superconducting nanowire single photon detector (SNSPD) setup, which was based on a microscope (IX73, Olympus) configuration (see Figure S5). For excitation, we used the output from a fiber coupled (FD7-PM, NKT Photonics) 77.88MHz pulsed continuum white-light laser (SuperK EXTREME EXB-6, NKT

Photonics) simultaneously delivering a set of wavelengths of 820 nm, 830 nm, and 840 nm by sending the continuum output through an acousto-optic tunable filter (AOTF; SuperK SELECT, NKT Photonics). The output of the fiber was expanded (BE05M-A, Thorlabs) and cleaned up by a single short-pass filter (FESH0900, Thorlabs). The excitation light was directed towards the microscope and was reflected by a 30:70 beam splitter (XF122, Omega Optical) and sent through an air objective (CPlanFLN 10x NA = 0.3). The objective focused the laser onto the sample and collected the luminescence. To block laser bleed-through, a long-pass filter was inserted in the detection path (FELH0900, Thorlabs). Because of the polarization sensitivity of the detector, we added a linear Glan-Thomson polarizer (GTHM10 Thorlabs) in the path (this is mainly for intensity calibration purposes where light from an unpolarized lamp is used).

The resulting emission was directed through a monochromator (SpectraPro 2300i, Princeton Instruments) and collimated before being focused down and directed towards a fiber launch system (MBT613D/M, Thorlabs) for coupling into a single mode fiber (ENI/1092976, Diamond). The fiber was then coupled into a cryogenic SNSPD system (ID281, IDQ). The single photon detection events were directed to a delay generator (DG535, Standford Research) to ensure that TTL pulses were fed to a single photon counting board (SPC-830, Becker & Hickl).
All SNSPD data was collected using LabVIEW. Official VIs from Becker & Hickl and Princeton Instruments were modified and combined and allowed for collecting time resolved emission maps; here, we only show the integrated decays or spectra. Wavelength and intensity calibrations were performed as previously described.[1] For calibrating the wavelength, we used selected wavelength outputs from our supercontinuum laser. Because of the SNSPD's large spectral range and the limited wavelength availability of our AOTF (690 – 1100 nm), we also used the second harmonics for calibration purposes. The intensity was calibrated using a calibration lamp (SL1-CAL, StellarNet Inc).

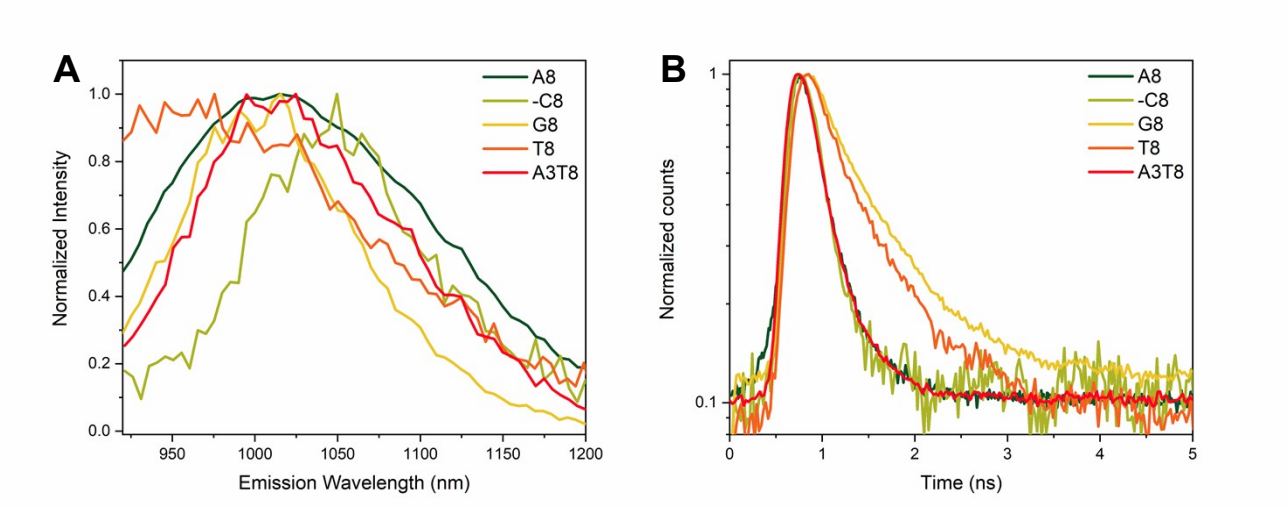

Figure S23. A) Emission spectra and **B)** fluorescence decay curves of the crystals of A8, -C8, G8, T8, and A3T8 mutants. The fluorescence was recorded with excitation wavelengths of 820, 830, and 840 nm, and the decays were obtained by summing the single photon counts between 920 nm and 1120 nm. The A8 mutant was integrated for 10 seconds per wavelength step, whereas -C8, G8, T8, and A3T8 were all integrated for 1 seconds to avoid the crystals drifting out of the measurement spot. The crystals were floating in the crystallization solution in the crystallization well.

5.3 Data collection, processing, phasing and refinement

To determine the structure of the T8 mutant, we collected datasets from BioMAX at MAX IV (Lund, Sweden). The diffraction patterns were obtained using 0.1° oscillation steps with an exposure time of 0.01 s at a wavelength of 0.7293 Å and with the beam set to 40% transmission. A total of 3600 frames were recorded. All datasets were processed with the program *XDS*.[5] The reflection data were converted by *Reflection file editor* of the *Phenix suite*.[6] The locations of 84 silvers, corresponding to three DNA-AgNC, were determined by the standard direct method phasing protocol in *SIR2019*.[7] The initial phase was estimated by the program *AutoSol* in the *Phenix suite*[6] using the location of the silvers as the reference heavy atom sites. The crystal structure was constructed by using the program *Coot*.[8, 9] The atomic parameters were refined using the program *phenix.refine* in the *Phenix suite*.[6] Crystal as well as the crystallization condition for the data collection, and the statistics of structure determination are summarized in Table S3 and Table S4, respectively.

Table S3. Crystallization conditions for X-ray diffraction data collection

Sample name	T8
Temperature	293K
DNA-AgNC solution (1 µl)	
DNA-AgNC T8	100-200 µM
Crystallization solution (1µl)	
Strontium nitrate	10 mM
Spermine	10 mM
3-(N-morpholino)propanesulfonic acid (pH = 7.0)	50 mM
2-Methyl-2,4-pentanediol	10%
Reservoir solution (250 µl)	
2-Methyl-2,4-pentanediol	40%
Crystals	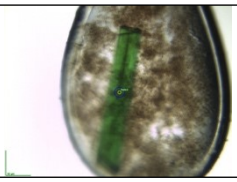

Table S4. Crystal data, statistics of data collection and structure refinement

PDB-ID code	9XRW, pdb00009xrw
Crystal data	
Space group	$P2_1$
Unit cell (Å, °)	a = 33.56, b = 108.11, c = 108.20, β = 90.03
Z [a]	8
Data collection	
Beamline	bioMAX of MAX IV
Wavelength (Å)	0.729319
Resolution (Å)	27.0-1.9
of the outer shell (Å)	1.95-1.90
Unique reflections	118688
Completeness (%)	98.6
in the outer shell (%)	98.5
R_{anom} [b] (%)	6.4
in the outer shell (%)	21.1
Redundancy	3.54
in the outer shell	3.56
Structure refinement	
Resolution range (Å)	27.0-1.9
Used reflections	118622
R-factor [c] (%)	13.8
R_{free} [d] (%)	15.6
Number of DNA atoms	5184
Number of Ag	2
Number of Cl	16

Number of Sr	11
Number of water	276
R.m.s.d. bond length (Å)	0.009
R.m.s.d. bond angles (°)	1.410

[a] Number of DNA-AgNC in the asymmetric unit.
[b] $R_{anom} = 100 \times \Sigma_{hklj}|I_{hklj}(+) - I_{hklj}(-)| / \Sigma_{hklj}[I_{hklj}(+) + I_{hklj}(-)]$.
[c] R-factor $= 100 \times \Sigma||F_o| - |F_c|| / \Sigma|F_o|$, where $|F_o|$ and $|F_c|$ are optimally scaled observed and calculated structure factor amplitudes, respectively.
[d] Calculated using a random set containing 10% of observations.

5.3.1 Crystal packing analysis

The eight subunits were aligned using the Kabsch algorithm,[10, 11] with the first subunit serving as the reference. After alignment, the atomic coordinates were averaged across all subunits to obtain a mean structure representing the average position of each atom. Root-mean-square-deviation (RMSD) values were then calculated between the averaged structure and each individual subunit to quantify deviations from the mean. For visualization purposes, the coordinates were translated to center each cluster at the origin (0, 0). Both the Kabsch alignment and RMSD calculations were performed using custom Python scripts.

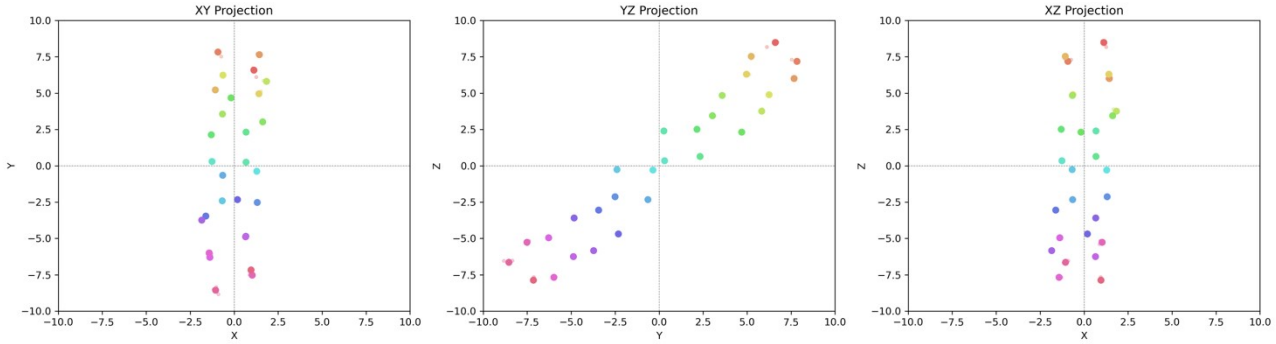

Figure S24. Superposition of the eight subunits in the asymmetric unit of the T8 crystal structure. Subunits are shown as semi-transparent circles, while filled circles represent the average position across all eight subunits. Colors are consistent across subunits and the averages to indicate the same silver atoms. Projections are shown, from left to right, onto the *XY*, *YZ*, and *XZ* planes.

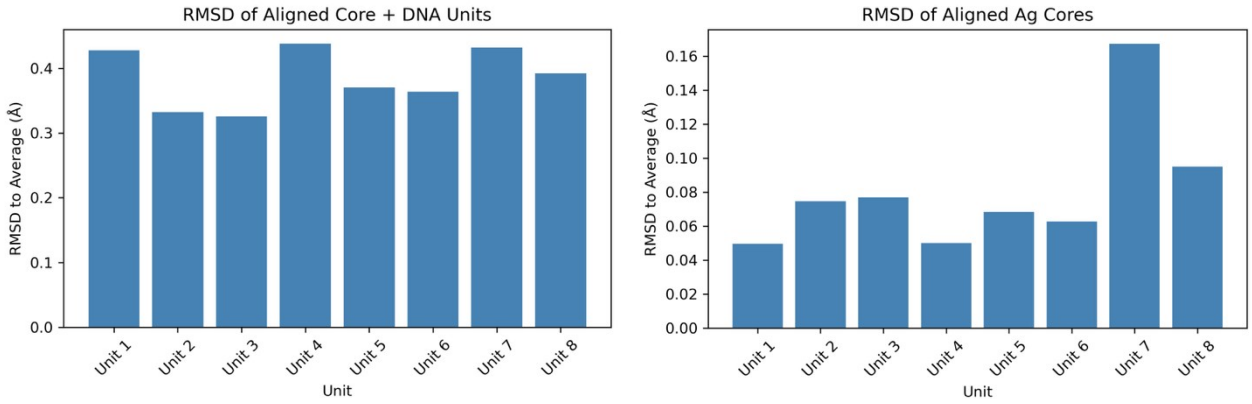

Figure S25. RMSD of individual subunits with respect to the average structure. **Left** panel includes both the metal core and the DNA strands. **Right** panel with only metal cores.

Author contributions.

Giacomo Romolini: Conceptualization, Data curation, Formal analysis, Funding acquisition, Investigation, Validation, Visualization, Writing - original draft, Writing - review & editing. **Hiroki Kanazawa**: Formal analysis, Methodology, Writing – original draft, Writing – review & editing. **Simon Wentzel Lind**: Formal analysis, Investigation, Methodology, Writing – review & editing**. Cecilia Cerretani:** Conceptualization, Formal analysis, Investigation, Supervision, Validation, Visualization, Writing - original draft, Writing - review & editing. **Christian Brinch Mollerup**: Resources, Validation, Writing – review & editing. **Letizia Liccardo**: Investigation, Validation, Writing – review & editing. **Zhiyu Huang**: Investigation, Writing – review & editing. **Leila Lo Leggio**: Funding acquisition, Resources, Supervision, Validation, Writing – review & editing. **Vanessa Rück**: Investigation, Writing – review & editing. **Jiro Kondo**: Funding acquisition, Methodology, Resources, Supervision, Validation, Writing – review & editing. **Tom Vosch**: Conceptualization, Formal analysis, Funding acquisition, Investigation, Resources, Supervision, Validation, Visualization, Writing - original draft, Writing - review & editing.

References.

1. M. B. Liisberg, Z. Shakeri Kardar, S. M. Copp, C. Cerretani and T. Vosch, *The Journal of Physical Chemistry Letters*, 2021, **12**, 1150-1154.
2. G. Romolini, H. Kanazawa, C. B. Mollerup, M. B. Liisberg, S. W. Lind, Z. Huang, C. Cerretani, J. Kondo and T. Vosch, *Small Structures*, 2025, **6**, 2500022.
3. A. M. Brouwer, *Pure and Applied Chemistry*, 2011, **83**, 2213-2228.
4. https://mstools.epfl.ch/deconvolution/
5. W. Kabsch, *Acta Crystallographica Section D*, 2010, **66**, 125-132.
6. D. Liebschner, P. V. Afonine, M. L. Baker, G. Bunkoczi, V. B. Chen, T. I. Croll, B. Hintze, L.-W. Hung, S. Jain, A. J. McCoy, N. W. Moriarty, R. D. Oeffner, B. K. Poon, M. G. Prisant, R. J. Read, J. S. Richardson, D. C. Richardson, M. D. Sammito, O. V. Sobolev, D. H. Stockwell, T. C. Terwilliger, A. G. Urzhumtsev, L. L. Videau, C. J. Williams and P. D. Adams, *Acta Crystallographica Section D*, 2019, **75**, 861-877.
7. M. C. Burla, R. Caliandro, B. Carrozzini, G. L. Cascarano, C. Cuocci, C. Giacovazzo, M. Mallamo, A. Mazzone and G. Polidori, *Journal of Applied Crystallography*, 2015, **48**, 306-309.
8. P. Emsley and K. Cowtan, *Acta Crystallographica Section D*, 2004, **60**, 2126-2132.
9. P. Emsley, B. Lohkamp, W. G. Scott and K. Cowtan, *Acta Crystallographica Section D*, 2010, **66**, 486-501.
10. W. Kabsch, *Acta Crystallographica Section A*, 1976, **32**, 922-923.
11. W. Kabsch, *Acta Crystallographica Section A*, 1978, **34**, 827-828.